

INFLUENCE OF SIZE EFFECTS ON STRUCTURAL PHASE TRANSITION AND DOMAIN STRUCTURE OF FERROELECTRIC NANO-SIZED BaTiO_3 RODS

NGUYEN VAN CHINH, NGUYEN THUY TRANG, BACH THANH CONG,
PHAN THI HONG NGAT

Computational materials science laboratory, Faculty of physics, Hanoi University of Science, Vietnam

Abstract. *In this paper, ab initio calculation on the BaTiO_3 quantum-rods was carried out in the framework of density functional theory (DFT) using local density approximation (LDA). While both LDA functional and gradient corrected versions underestimated the optical gap of the bulk BaTiO_3 , the LDA ones resulted in the better fit with experimental data. The shape ratio of the rods varied from 1:10 to 1:1 for single unit cell cross-section rods (SURs) and from 2:10 to 2:2 for double unit cell cross-section rods (DURs). Each rod ended at BaO plane or TiO_2 plane. One of the most interesting observations obtained from the calculation was the structural-phase transition along the rods which has been addressed as the smeared phase transition in literatures. Besides, the mean values of $c:a$ which were averaged over unit cells of each rod showed the stability of the tetragonal phase for BaO ended SURs (type A1) with length above 1.6 nm. For BaO ended DURs (type A2), the tetragonal phase was shown to be stable at length above 1.3 nm. These two lengths can be considered as the cubic-tetragonal transition lengths. The structural-phase transition did not occur for the TiO_2 ended SURs (type B1) and DURs (type B2) at any length up to 3.2 nm. Reduction of the interaction energy between surface charges stimulates a formulation of 180° domain wall at the middle of each rod of all types. Additionally, there are an anomalous flipping of the electric dipoles at the ends of the A2 rods.*

I. INTRODUCTION

Ferroelectric materials offer great potential for next generation high density storage devices, such as nonvolatile random memory access and high strain actuators in microelectro mechanical systems applications due to their inherent high dielectric properties and high strain response [11, 13].

Previous research about BaTiO_3 nanowires as of author Geneste et al [17] have shown us the finite-size effects in BaTiO_3 nanowires. The ferroelectric instability exhibits a marked chain-like character so that, in nanowires, it could a priori be preserved down to very small sizes. But author G. Pilia et al [3] based on the first-principles had studied about ferroelectric properties of nanowires and then has shown the size limit that has ferroelectric properties with polarized along wire is about $12A^0$ at 0^0 K. Here we present about influence of size effects on structural phase transition and domain structure of ferroelectric nano-sized BaTiO_3 rods. The 180° domain wall structure J. Padilla et al [16] just research on the bulk material and show that energy of domain wall is about 15.8 (erg/cm^2), but for bulk material PbTiO_3 this value is much greater, about 0.15 (J/m^2). This paper is organized as follows. In Sec.II we describe the technical details of our

computational method and the geometry of the super cells used to model calculations. In Sec.III we present our results on the lattice constants, local ferroelectric distortions and calculations structure 180° domain wall. Finally, the paper concludes with a summary.

II. COMPUTATIONAL METHODS

Calculations have been carried out with the Dmol³ package within the framework of the density-functional theory [1] using the Local Density Approximation (LDA) with correlation functional by Perdew, J. P.; Wang, Y. PWC [2]. The atoms have been described by all-electron relativistic basic sets DNP. The crystal structure of BaTiO₃ has space group Pm(3)m, figure (1) shows the unit cell. From the cubic unit cell of BaTiO₃, we constructed four models (see Fig.2). The shape ratio of the rods is varied from 1:10 to 1:1 for single unit cell cross-section rods (SURs) and from 2:10 to 2:2 for double unit cell cross-section rods (DURs). Each rod ends at BaO plane or TiO₂ plane. For example, nano rod of BaTiO₃ that ends at BaO plane and SURs are given a name type A1. Moreover, BaO that ends at DURs is type A2. Similarly, TiO₂ that ends at SURs or DURs are type B1, type B2 respectively. We used quantum calculations for these four models. All DFT

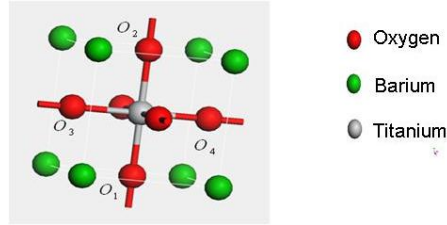


Fig. 1. The cubic unit cell of BaTiO₃.

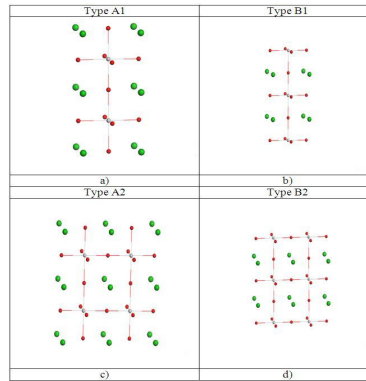


Fig. 2. Nano rod models of BaTiO₃ ending at BaO SURs, BaO DURs, TiO₂ SURs, TiO₂ DURs correspond to type A1, type A2, type B1, type B2. Their length is two unit cell (2U).

calculations presented in this work happen at O^0 K.

III. RESULTS AND DISCUSSION

III.1. Lattice structure

BaTiO₃ nanowires after minimized configuration we calculate the average constant of wires a (along the axis x), b (along the axis y), c (along the axis z). With nanowires of A1 and B1, then $a = b$ by symmetric properties of the system. Characterize the phase transition from cubic to tetragonal phase, we introduce characteristic ratio c/a [4, 5]. If ratio $c/a \geq 1.01$, we have tetragonal phase in the material. The phase transition from cubic to tetragonal phase is gradual transition, the phase transition happens from the internal wire to the outer wire. In the wire type A1, the phase transition occurs at $\geq 5U$ wire length (about $16 A^0$). But when increasing size up to A2 wire surface, the phase transition occurs earlier, just at $4U$ of wire length. This does not happen in the wire type B1, the phase transition does not occur even if the wire surface is type B2. This may explain that the properties of BaTiO₃ nanowire is under the influence of effect size [6]. Tetrag* symbol is the value measured experimentally of BaTiO₃ in the tetragonal phase [7]. Seeing that at the value $6U$ of wire A1, the c/a ratio by *ab initio* calculations coincide completely with the experimental value. In Fig.3 magenta dotted line showing the c/a ratio of the bulk

Table 1. Computed values of structural parameters for BaTiO₃. Where a and c are lattice constants of nanowires type A1, type B1.

Terminated	<i>1BaO</i>			<i>1TiO₂</i>		
Lattice constants	a	c	c/a	a	c	c/a
1U	3.884	3.884	1.000	4.000	3.427	0.857
2U	3.901	3.918	1.004	3.965	3.705	0.934
3U	3.908	3.937	1.007	3.951	3.800	0.962
4U	3.911	3.948	1.009	3.962	3.847	0.971
5U	3.913	3.954	1.010	3.939	3.875	0.984
6U	3.914	3.959	1.011	3.937	3.893	0.989
7U	3.916	3.963	1.012	3.935	3.906	0.993
8U	3.917	3.968	1.013	3.933	3.916	0.996
9U	3.918	3.970	1.013	3.762	3.780	1.005
10U	3.919	3.968	1.013	3.762	3.786	1.006
Bulk	4.010	4.010	1.000			

material, dark yellow solid line showing the ratio $c/a = 1.01$ is limited to a tetragonal phase. Through pictures, we can see that the larger the size of BaO surface is, the faster the phase transition is, the phase transition can observe more clearly in the wire A2. In contrast, the wires type B1 and B2 phase transition is very unlikely.

III.2. Local distortions ferroelectric

An important property of BaTiO₃ ceramics are electrical properties, which was brought from the position deviation on Ti atoms in TiO₂ octaheron. This property is

Table 2. Computed values of structural parameters for BaTiO₃. Where b, a and c are lattice constants of nanowires type A2, type B2.

Terminated	<i>2BaO</i>				<i>2TiO₂</i>			
Lattice constants	b	a	c	c/a	b	a	c	c/a
2U	7.868	3.910	3.931	1.005	7.982	3.982	3.681	0.924
3U	7.881	3.916	3.948	1.008	7.954	3.962	3.784	0.955
4U	7.593	3.772	3.820	1.013	7.616	3.786	3.724	0.984
5U	7.597	3.771	3.828	1.015	7.788	3.867	3.745	0.968
6U	7.598	3.770	3.832	1.016	7.618	3.784	3.747	0.990
7U	7.602	3.770	3.836	1.018	7.619	3.782	3.762	0.995
8U	7.604	3.771	3.839	1.018	7.618	3.780	3.777	0.999
9U	7.606	3.771	3.841	1.019	7.618	3.779	3.783	1.001
10U	7.607	3.771	3.842	1.019				
Bulk	8.020	4.010	4.100	1				
Tetrag*		3.992	4.036	1.011				

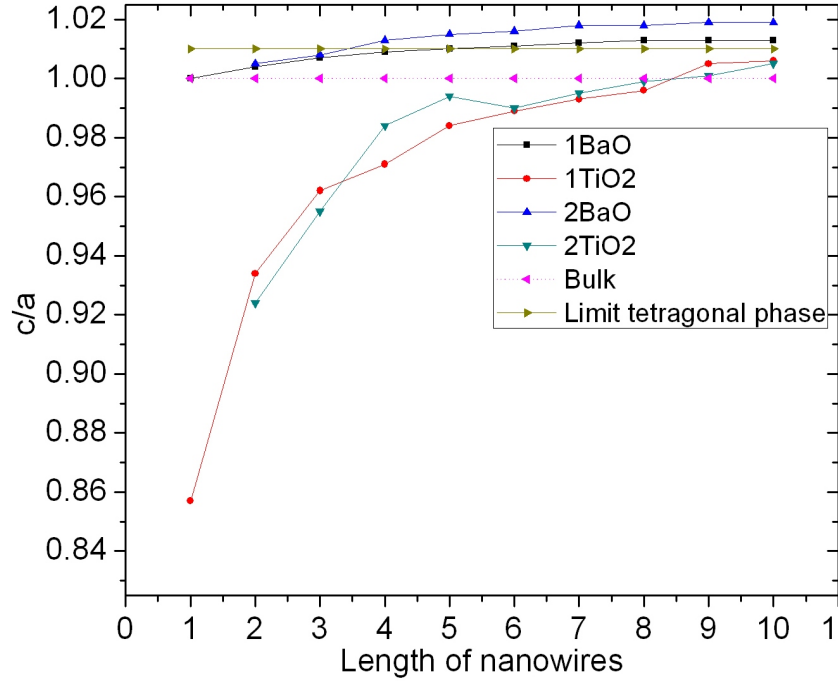


Fig. 3. Nano rod models of BaTiO₃ ending at BaO SURs, BaO DURs, TiO₂ SURs, TiO₂ DURs correspond to type A1, type A2, type B1, type B2. Their length is two unit cell (2U).

characterized by equation[8]

$$\begin{cases} d_x = x_{O1} + x_{O2} - 2x_{Ti} \\ d_y = y_{O1} + y_{O2} - 2y_{Ti} \\ d_z = z_{O1} + z_{O2} - 2z_{Ti} \end{cases} \quad (1)$$

When we have not been maximized the configuration $d_x=d_y=d_z$. After we maximized configuration, because we consider the loss of circulation of the wire along the z axis so we pay attention to d_z , with z_{O1} , z_{O2} , z_{Ti} the coordinates of oxygen 1 atom, oxygen 2 and Ti in the unit cell, respectively (see Fig.1). Origin is taken from the heart wires, which are numbered 0,1,2, ... corresponding to class 0, 1, 2 ... of the unit cell (see Fig.3). In Fig.5

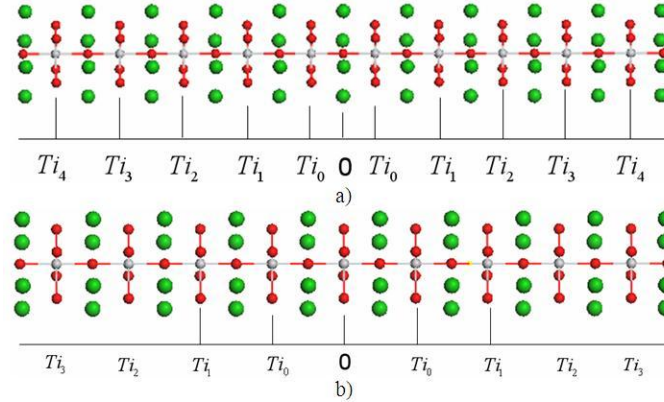


Fig. 4. BaTiO₃ nanowires of type A1 with 10U (origin of coordinates is Oxygen in central layer) a) and 9U length (origin of coordinates is Titanium in central layer) b).

we introduce local ferroelectric distortions for each unit cell of the nanowires. Because the properties of each wire geometry with different cutting surfaces are different thus we draw local ferroelectric distortions for each unit cell (the equivalent details each location of Ti on the nanowires). For BaTiO₃ nanowires in the form of type A1, vector of the local

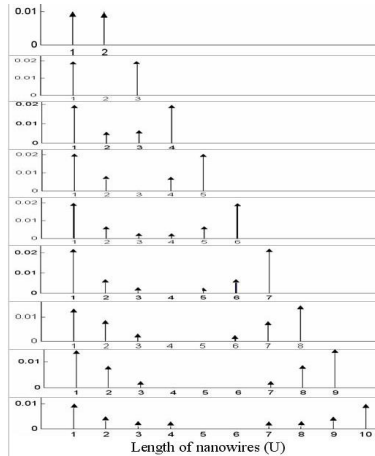


Fig. 5. Specified deformation local ferroelectric properties for each position along the length of Ti wire with the kind of type A1.

ferroelectric distortions detail for each position along the length of wires. With the arrow

pointing up, we have value algebra by the formula (1) carry positive sign (+). When arrows go down, we have value algebra by the formula (1) carry negative sign (-). Vector of the local ferroelectric distortions have common properties such as ferromagnetic materials. At half the length of wire connection distance between Ti and O are the same sign. Magnitude is the biggest in boundary and which decline to go into the heart nanowires. When the length is odd for example, $3U$, $5U$,...the deviation of Ti at the center is 0. This is only true for even-length nanowire when length is large enough above 3.7nm . With wire length $7U$, the deviation of Ti from the outside is the largest about $0.021 A^0$ and is the smallest at wire length $10U$ about $0.008 A^0$. This nanowires take form domain wall but which have not reversal of the Ti. When wire length is long enough, the deviation of the Ti center isn't significant. For example with wires length $9U$ and $10U$, the deviation of the Ti is equal to 0. When we consider a half-length nanowire, direction of the vector local ferroelectric

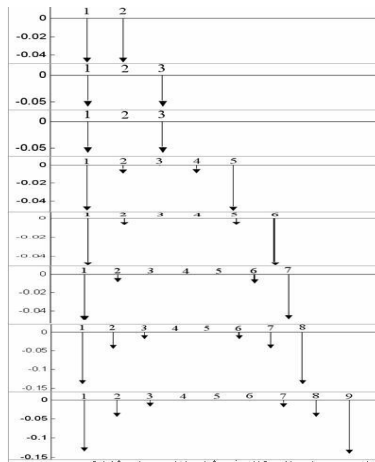


Fig. 6. Specified ferroelectric local deformation for each position along the length of Ti wire of type B1.

distortions is always downward in the wire type B1. Like wire type A1, magnitude of the deviation the Ti atoms are minimum at center. Deviation of the Ti outside wire $10U$ about $0.131 A^0$, which is maximum. This deviation increases from $3U$ to $10U$. When we consider wire type A2, the length of wire is shorter $12A^0$, we do not find the reversal of surface Ti. This result is similar to the type A1 and type B1. However, the length of wire is longer $16A^0$ (from $4U$ to $10U$) we still find the reversal of surface Ti with type A2. This means all Ti atoms directions toward the center, except the surface Ti atom. So different surface BaTiO_3 nanowires have different properties. For example, we can observe domain walls and the flip of surface Ti with $6U$ wire (see Fig.9). This result is very new and attractive. We compare the deviation of Ti position by measuring the angle $\widehat{O_3TiO_4}$. Where O_3, O_4 are oxygen atoms, which appertain parallel plane with the Oz axis. Vector of deformation local ferroelectric properties specified for each position along the length of Ti wire of type B2, which have similar property wire type B1. Length of nanowire is an even number unit cell, the deviation of center Ti is equal to 0. The deviation of selvedge Ti atom is

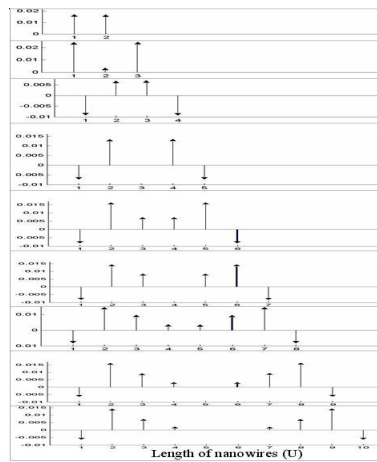


Fig. 7. Local ferroelectric deformation specified for each position along the length of Ti wire type A2.

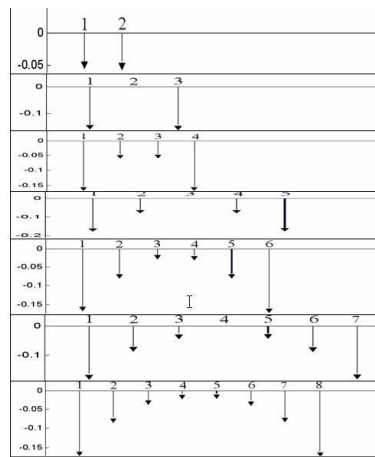


Fig. 8. Deformation local ferroelectric properties specified for each position along the length of Ti wire of type B2.

maximum, which decrease in the center nanowire. When we consider the wire of type A1, type B1 and type B2, we do not find capsizes of the surface Ti. This matter only occurs in the wire type A2, indicating of the influence of size effects in BaTiO₃ nanowires.

III.3. Structure of 180° domain wall

Domain walls as in theory and experiment have found and demonstrated by atomic force microscopy (AFM) and piezoresponse force microscopy (PFM) [14] images captured In Fig.9 we can see the wall domain 180° are formed inside with the same 6U length type wires of all different type A1, type B1, type A2, type B2. Particularly in A2 type wires, there is a reversal of the surface Ti atoms. In all types of wires domain walls 180° are of the form (see Fig.10) the results obtained similar with [9, 10, 15, 16].

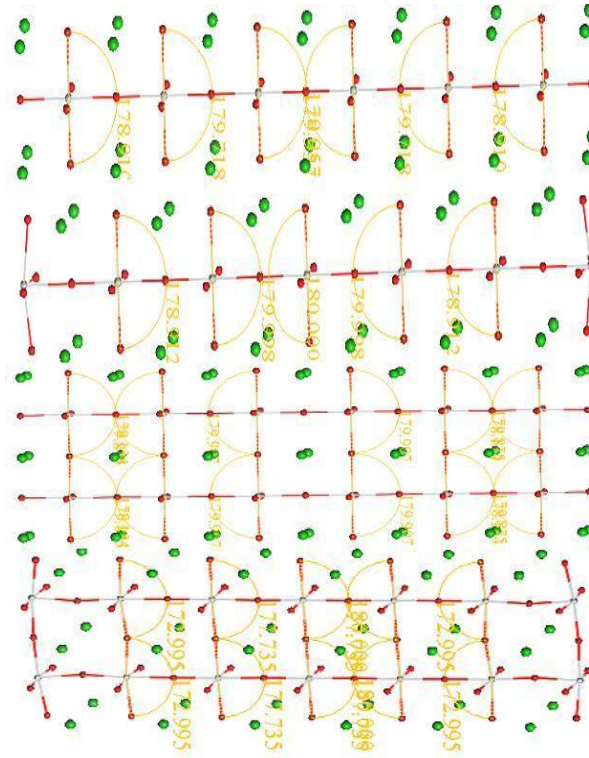


Fig. 9. Images about the deviation of Ti atoms through corners $\widehat{O_3TiO_4}$ and walls domain 180° of 6U length type wires with corresponding type A1, type B1, type A2, type B2 nanowires.

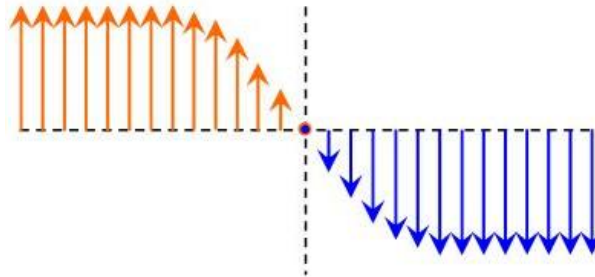


Fig. 10. Image of 1800 domain walls formed in the nanowires.

IV. SUMMARY

In this paper we have found a transformation of cubic to tetragonal phase in the wire type A1 and type A2. The phase transition occurs more easily in the wire of type A. For example, even just 4U length of A2 type wires has tetragonal phase. While in the wire type A1 required the minimum length 6U. In addition, we obtained the deformation

of local ferroelectric properties detailed for each position of Ti. These results have in common is the deviation of the outermost Ti is the largest and decrease when into center of nanowires. Particularly with the string type A2, the surface Ti atoms reverse when string length greater than 1.6 nm. Finally, the pictures of domain wall 180° have found.

V. ACKNOWLEDGMENT

The authors gratefully acknowledge the NAFOSTED grant 103.02.111.09 for financial support.

REFERENCES

- [1] R. G. Parr, W. Yang, *Density-Functional Theory of Atoms and Molecules*, 1989 Oxford University Press, New York.
- [2] J. P. Perdew, Y. Wang, *Phys. Rev. B* **45** (1992) 13244.
- [3] G. Pilania, S. P. Alpay, R. Ramprasad, *Phys. Rev. B* **80** (2009) 014113.
- [4] W. Tian, J. C. Jiang, X. Q. Pana, *Appl. Phys. Lett* **89** (2006) 092905.
- [5] F. Jona, G. Shirane, *Ferroelectric Crystals*, 1962 Macmillan, New York.
- [6] G. Geneste, E. Bousquet, J. Junquera, P. Ghosez, *Appl. Phys. Lett* **88** (2006) 112906.
- [7] B. Cord, R. Courths, *Surf. Sci* **152/153** (1985) 1141.
- [8] G. Pilania, S. P. Alpay, R. Ramprasad, *Phys. Rev. B* **80** (2009) 014113.
- [9] S. Pöykkö, D. J. Chadi, *Appl. Phys. Lett* **75** (1999) 18.
- [10] J. Padilla, W. Zhong, David Vanderbilt, *Phys. Rev. B* **53** (1996) 5969 (R).
- [11] A. I. Kingon, J. P. Maria, S. K. Streiffer, *Nature* **406** (2000) 1032 (London).
- [12] D. L. Polla, L. F. Francis, *Annu. Rev. Mater. Sci* **28** (1998) 563.
- [13] K. Bhattacharya, G. Ravichandran, *Acta Mater* **51** (2003) 5941.
- [14] C. Franck, G. Ravichandran, K. Bhattacharya, *Appl. Phys. Lett* **88** (2006) 102907.
- [15] B. Meyer, D. Vanderbilt, *Phys. Rev. B* **65** (2002) 104111.
- [16] Rakesh K Behera, Chan Woo Lee, Donghwa Lee, Anna N. Morozovska, Susan B. Sinnott, Aravind Asthagiri, Venkatraman Gopalan, Simon R. Phillpot, *J. Phys.: Condens. Matter* **23** (2011) 175902.
- [17] Grgory Geneste, Eric Bousquet, Javier Junquera, Philippe Ghosez, *Appl. Phys. Lett* **88** (2006) 112906.

Received 30-09-2011.